# A ROBUST SUPERCRITICAL GEOTHERMAL SIMULATOR

John O'Sullivan[1], Juliet Newson[2], Sam Alcaraz[3], Sam Barton[2], Richmond Baraza[4], Adrian Croucher[1], Samuel Scott[2] and Mike O'Sullivan[1]

[1]Department of Engineering Science and Geothermal Institute, University of Auckland, New Zealand

[2]Iceland School of Energy, Reykjavik University, Iceland

[3]GNS Science, Wairakei Research Centre, Private Bag 2000, Taupo 3352, New Zealand

[4]Geothermal Development Company, Kenya

jp.osullivan@auckland.ac.nz

**Keywords:** *Geothermal modelling, supercritical, Menengai, Reykjanes, Krafla, Taupo volcanic zone*

**ABSTRACT**

Recent improvements to a supercritical equation-of-state (EOS) for the simulator TOUGH2 are discussed together with its application to simulations of Menengai (Kenya), Reykjanes Peninsula (Iceland), Krafla (Iceland) and the TVZ (New Zealand). The models of Reykjanes Peninsula and the TVZ include multiple geothermal systems.

The new EOS uses smoother and more reliable transitions into and out of the supercritical region than our previous supercritical EOS. This allows natural state simulations to converge robustly, thus enabling models to be calibrated effectively.

An air/water equation-of-state, similar to EOS3 in TOUGH2, but with supercritical capability is also described. This new EOS3sc allows simulation of regions including the shallow unsaturated zone and extending deep to the high-temperature and high-pressure zone.

## 1. SUPERCRITICAL GEOTHERMAL SIMULATORS

Several supercritical simulators have been developed in the past including HYDROTHERM (Hayba and Ingebritsen, 1994), the HOTH2O extension to the STAR simulator (Pritchett, 1995) and CSMP++ (Weis, *et al*. 2014; Driesner et al., 2015). Brikowski (2001) and Kissling (2004) both developed supercritical equations-of-state for TOUGH2 and Croucher and O'Sullivan (2008) developed a supercritical equations-of-state for AUTOUGH2 (Yeh *et al*., 2012), the University of Auckland's version of TOUGH2 (Pruess et al., 1999). The algorithm developed by Croucher and O'Sullivan (2008) was recently implemented in the standard version of TOUGH2 by Magnusdottir and Finsterle (2015).

The Croucher and O'Sullivan (2008) supercritical equations-of-state (called here EOS1sc) was based on the thermodynamic regions defined in the IAPWS-97 Formulation (Wagner *et al*., 2000) for calculating thermodynamic properties.

Despite these advances, there are very few examples of full-scale, three-dimensional simulations of geothermal systems with supercritical conditions present. Scott et al. (2015a, 2015b, 2016, 2017) used CSMP++ to simulate supercritical geothermal resource formation around magmatic intrusions, but only with two-dimensional models.

In the case of the TOUGH2 family of simulators, there are well-known convergence issues that often occur during phase changes (O'Sullivan *et al.*, 2013, O'Sullivan *et al.*, 2014). A supercritical equation-of-state contains many more possible phase changes than a subcritical equation-of-state and hence many more convergence issues may arise. In this article we first discuss improvements made to the EOS1sc equation-of-state to ensure smoother transitions between different thermodynamic regimes and then discuss the inclusion of air in the supercritical EOS. The air water EOS in TOUGH2 is called EOS3 and so we call the supercritical version EOS3sc. Finally, we discuss the application of EOS1sc and EOS3sc to studies of real geothermal systems.

## 2. IMPROVEMENTS TO EOS1sc

The IAPWS-97 Formulation (Wagner *et al*., 2000) for calculating thermodynamic properties defines four thermodynamic regions: 1 liquid, 2 vapour, 3 supercritical and 4 two-phase. These regions are shown on a pressure-temperature plot in Figure 1a and on a density temperature plot in Figure 1b.

The boundaries defined for the thermodynamic calculation regions identify where different independent variables are used for the thermodynamic formulae. Within the supercritical region (region 3 in Figure 1a) the thermodynamic properties are calculated using formulae dependent on density and temperature whereas in regions 1 and 2 they are calculated using formulae dependent on pressure and temperature. In their original algorithm Croucher and O'Sullivan (2008) introduced the idea of a supercritical phase and a change in phase when crossing into region 3 and as part of the process changed the primary solution variables from pressure and temperature to density and temperature. Unfortunately, there are very small but significant discontinuities in the thermodynamic properties calculated by the different formulae used in regions 1 and 2 and those used in region 3.

These discontinuities did not cause any problems with the test cases used by Croucher and O'Sullivan (2008) to check their version of EOS1sc. However, in subsequent simulations we found difficulty with convergence of some natural state simulations. To overcome this problem, we subdivided region 3 and moved the 1/2 and 2/3 boundaries by a small amount. The new regions are shown in Figure 2.

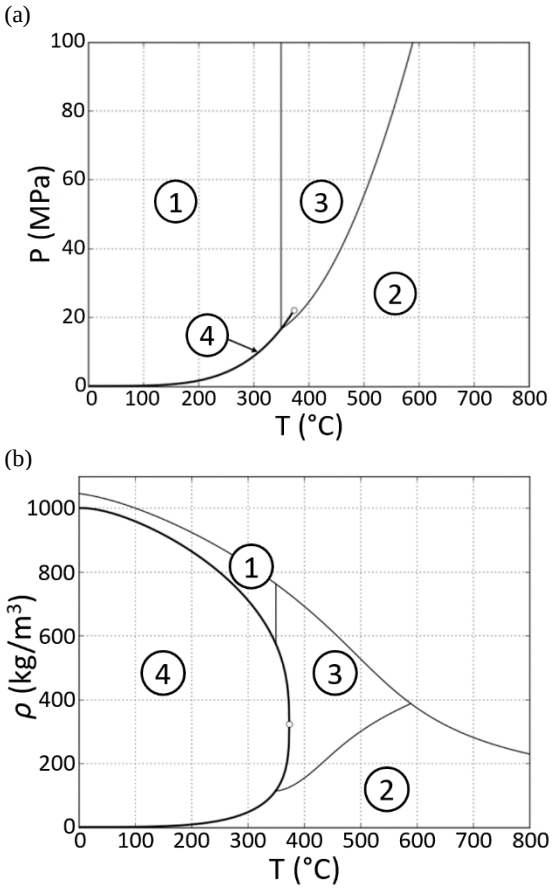


**Figure 1: IAPWS-97 thermodynamic regions (a) pressure-temperature, (b) density-temperature.**

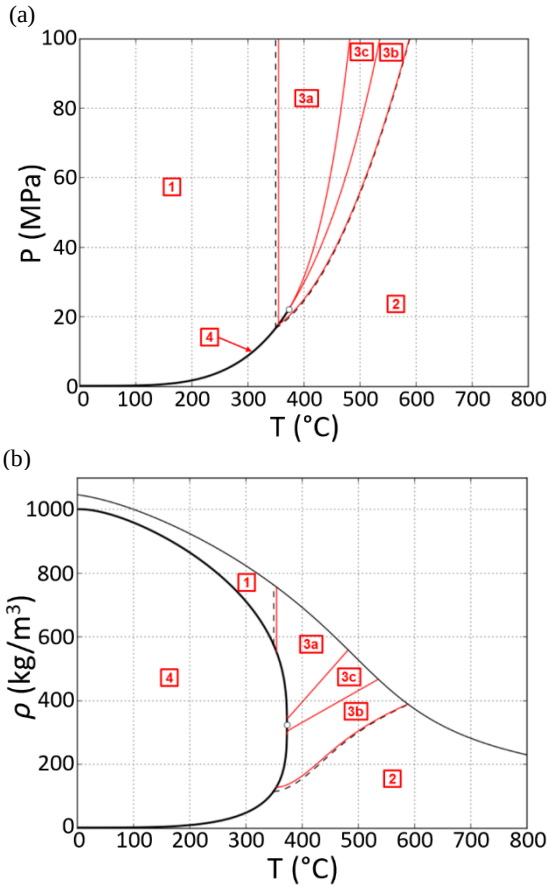


**Figure 2: Modified thermodynamic regions (a) pressure-temperature, (b) density-temperature.**

The choice of primary variables in each subregion and the smoothing applied to ensure continuity across all 13 boundaries between regions are discussed in more detail in O'Sullivan et al. (2016).

Figure 2 shows a "transition" zone (3c) in the supercritical region which allows for a smooth transition from a "liquid-like" (3a) to a "vapour-like" (3b) supercritical fluid. Zone 3c also includes the critical point at which derivative thermodynamic quantities such as heat capacity and compressibility become singular and special care is required to deal with the critical point (see O'Sullivan et al., 2016).

The boundaries of zone 3c have been defined for numerical reasons and are somewhat arbitrary. This issue is also discussed by Driesner et al. (2016). Also, there are some physical arguments for the existence of this type of zone (Brazhkin and Trachenko, 2012) and the boundaries could be adjusted accordingly.

## 3. DEVELOPMENT OF EOS3sc

In order to model geothermal systems from the surface down to the brittle-ductile transition zone, the EOS must be able to handle both supercritical conditions at depth and the unsaturated vadose zone near the surface. In standard TOUGH2 this can be achieved by using the EOS3 equation-of-state, which includes air as an additional component in the governing equations. Including air with the supercritical EOS could be achieved in several ways. One approach could be to only include air in the shallow zones of the model and track an internal boundary with the rest of the domain where only pure water exists. However, determining the depth to which air is transported would be challenging as would handling an internal boundary.

In our development of a supercritical version of EOS3 (called EOS3sc) we include air throughout the domain, accepting that the mass fraction of air will be very small at depth and careful treatment will be required to ensure the mass of air is conserved. In EOS3 the air is treated as a passive scalar in the liquid phase but contributes to the enthalpy, viscosity and density of the vapour phase (O'Sullivan *et al.*, 2013). To ensure consistency with this approach in EOS3sc, air is treated as a passive scalar in the "liquid-like" supercritical region but contributes to the enthalpy, viscosity and density of the "vapour-like" phase.

The introduction of air further complicates the transitions between the thermodynamic regions. Details are given in O'Sullivan et al. (2016).

## 4. MENENGAI

The first application of EOS3sc to a real geothermal system was our modelling study of Menengai, Kenya (O'Sullivan et al., 2015). Located in the Great Rift Valley in Kenya, Menengai Crater is a massive shield volcano with one of the largest calderas in the world. Leat (1984) describes the caldera as a major topographical feature of the Great Rift Valley and the best-preserved Krakatau-style caldera in the world. Following Olkaria, the geothermal field hosted within the caldera is the second in Kenya to be investigated for

development, with surface exploration beginning in 2004 (Kipyego *et al.*, 2013). Since 2011 over 50 exploration wells and production wells have been drilled with maximum temperatures recorded in excess of 390ºC, demonstrating the potential of the field for energy production and indicating that it probably contains supercritical fluid.

Our first modelling study of Menengai (Kipyego *et al.*, 2013) used the standard version of AUTOUGH2 with the EOS3 equation-of-state. This model was clearly unsatisfactory because it could not cope with the high temperatures measured at Menengai and we subsequently carried out a second study using EOS3sc (O'Sullivan *et al.*, 2015).

As shown in Figure 3, the model was relatively coarse but was able to produce a reasonable match to the measured downhole temperature profiles (see Figure 4). The supercritical model significantly improves the match to the downhole temperatures for these two wells (and for some of the other wells – not shown).

The supercritical model was then used to simulate three potential future production scenarios and the results were compared with those obtained using the standard model (O'Sullivan *et al.*, 2015). The results show that with a model that accurately represents the high temperatures and supercritical conditions in the Menengai system, approximately 30% more steam is produced than is predicted by the standard model running the same scenario. Such a large difference in the predictions highlights the need for modelling the high-temperature conditions in the system accurately using supercritical modelling techniques.

Recently, the Menengai model has been updated using an improved geological model, a higher resolution grid and includes an explicit representation of the magma bodies under the Menengai caldera and the Ol' Rongai field (Baraza and O'Sullivan, 2020). The new model uses a different approach for calibrating the deep geothermal input by fixing the surface temperature of the magma bodies to 450°C and then making small adjustments to their depth and location (a similar approach was used for the model of Reykjanes Peninsula discussed below). The depths and locations of the magma bodies are constrained by the gravity data presented by Kanda et al. (2019).

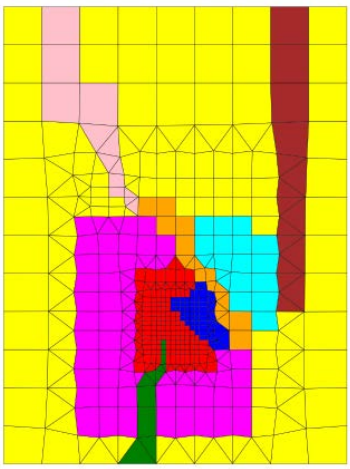

**Figure 3: Plan view of rock-types in the Menengai model, including faults and caldera structures.**

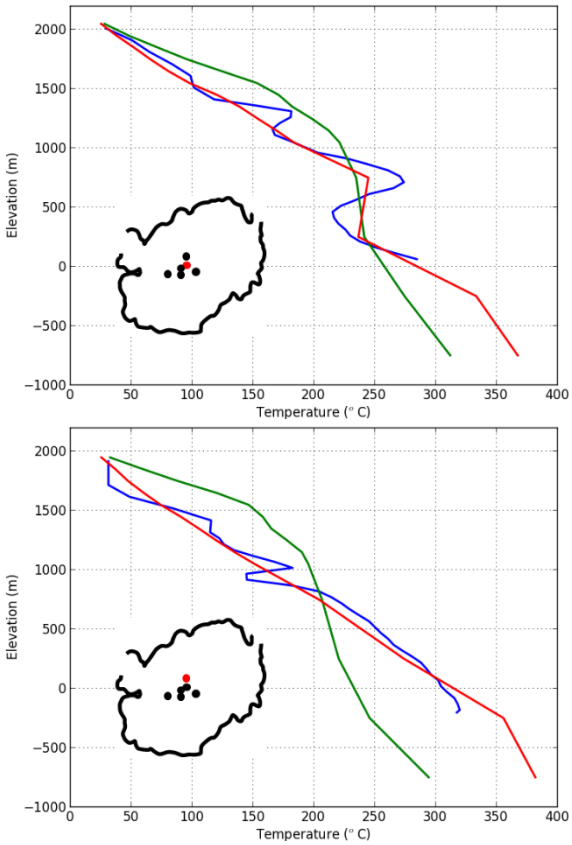


**Figure 4: Downhole temperatures for two Menengai exploration wells. Measured data shown in blue, supercritical model results in red, and standard model results in green. Location of each well within the caldera is indicated with a red dot.**

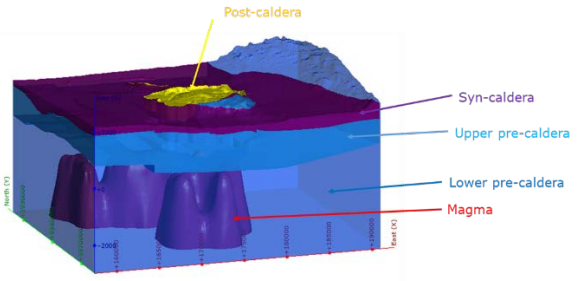


**Figure 5: The new geological model of the Menengai geothermal system including the magma bodies field (Baraza and O'Sullivan, 2020).**

## 5. REYKJANES PENINSULA

The Reykjanes Peninsula, located in the south-west of Iceland, is an on-land extension of the mid-Atlantic ridge, a divergent plate boundary. Its surface geology is characterised by extensive sub-aerial lava flows with hyaloclastite formations as key surface features. It is home to two geothermal power plants known as Reykjanes and Svartsengi which have over 50 years of exploration and utilisation history. It is also the location of an exploratory deep well known as IDPP2, which forms part of a project aimed at testing the economic feasibility of extracting energy and chemicals out of hydrothermal systems at supercritical conditions.

### 5.1 Conceptual model

A set of clear modelling objectives guided the development of the regional conceptual model. These objectives can be summarised as follows:

i. Provide a combined profile of the topography and bathymetry of the region capturing the top boundary effects of meteoric and seawater ingress.
ii. Develop an appropriately simplified lithology of the Reykjanes peninsula which encapsulates the Reykjanes, Eldvörp and Svartsengi geothermal fields which sit along a divergent plate boundary
iii. Map trends and zones of highly permeable structures across the region based on the location of faults, fissures and areas of high seismic activity.
iv. Map out the clay caps of the known geothermal fields.
v. Create a central repository of geological and geophysical information in graphical format including geological maps and cross sections, resistivity surveys and well logs.

Leapfrog software was used to develop the 3D regional conceptual model and acted as the main repository of graphical geological information. The conceptual model was developed in three steps: first, the stratified lithological layers were created utilising a simplified lithology, secondly permeable structures were identified in the region, and finally, the clay caps over the known geothermal fields were developed.

### 5.2 Geological model

Five main lithological units were chosen to represent the stratigraphy of the region. In the context of this model they are known as post-glacial lava (L), hyaloclastite (H), pillow lava (P), extrusive-intrusive transition zone (T) and the sheeted dike complex (D). These are names used in this study to summarise a range of formations and are representative of the volcanic history over time. These lithological categories can be summarised as follows:

*Post-Glacial Lava* - represents any formation that formed in the Holocene epoch less than 12.000 years ago. This mainly represents sub-aerial lava flows from eruptive fissures and shield volcanoes in the region.

*Hyaloclastite* - represents formations that formed during the late Pleistocene epoch during glaciation and so is characterised by sub-glacial eruptions and low-depth sub-marine eruptive formations forming tuff. These formations are visible today as mountains and large hills along the current plate boundary.

*Pillow Lava* - represents the formations that formed before Iceland had risen above sea level and was in contact with very thick layers of glacial ice or formed during the earlier Pleistocene epoch. These formations formed at depth beneath the sea with pillow lavas representing one of the extrusive formations that can be found at a divergent plate boundary. It must be recognised that pillow lava can also form at the base of a hyaloclastite formation in more recent sub-glacial eruption.

*Extrusive-intrusive transition* - represents formations where the frequency of intrusive dykes and sills begins to rapidly increase. This is typical of the subsurface geology of the region as more recent volcanic activity along the rift zone results in intrusives travelling from depth through existing formations to form new formations above.

*Sheeted Dike Complex* - represents the formations at depth that have been intruded by many dykes (normally dolerites) and act as feeders for overlaying extrusive formations above. This formation category also represents the bottom of the hydrothermal cells as the brittle-ductile boundary is approached and is characterised by rapid increases in temperatures and reduced permeability. This lithological category will be used to set the initial bottom boundary isotherm as further explained in the numerical model setup.

The peninsula contains many visible faults and fractures, with some of them providing vertical permeability for known geothermal systems. The conceptual model is too large to capture all the structures. A novel approach was developed inspired by Khodayar et al (2018). Rather than tracing out individual structures, structural trends were identified across the region by tracing out apparent trends in faults and fissures in the region. These trends had a NE-SW strike and in general were at an oblique angle to the plate boundary, consistent with tectonics of the area. An emphasis was placed on creating trends along or over existing visible hyaloclastite formations. Subsequently seismic maps were used to map out the extents of the rift zone at the north and south of the model and to identify those sections of the structural trends which were most seismically active.

The clay caps were developed from a combination of hydrothermal alteration lithology profiles and TEM and MT resistivity surveys. The surveys in cross-section and aerial map form were used to develop the shape of the clay caps in Leapfrog. The TEM and MT resistivity surveys were taken from De Freitas et al. (2018) who used a similar methodology to identify the location of the cap rock while creating a numerical model of the Svartsengi geothermal reservoir.

### 5.3 Numerical model

A relatively coarse regular rectangular model was set up, consisting of 55,468 blocks. Smaller blocks were used near the geothermal systems and thinner layers were used in the shallow zone. The model grid and the rock-types are shown in Figure 6.

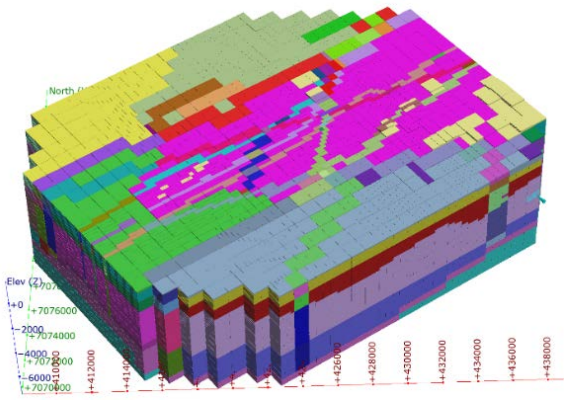


**Figure 6: Grid for the model of Reykjanes Peninsula**

A natural state simulation was carried out with this model using AUTOUGH2 with EOS3sc.

### 5.4 Calibration

Conceptually the Reykjanes plate boundary is underlain by a sheeted dyke complex which hosts a multitude of hot intrusive bodies as opposed to isolated chambers of magma. This can be approximated as a constant temperature conductive body with a topography defined by the history of volcanic activity in the region. The sheeted dike complex was used to initially set the topography of this isothermal surface. shown in Figure 7 as the orange layer. This is a novel approach that allows the whole iso-surface to be adjusted to match the temperatures in the geothermal systems.

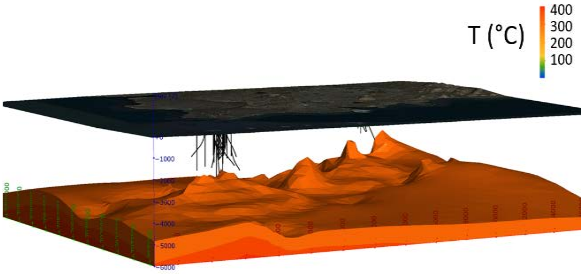


**Figure 7: Constant temperature iso-surface at the base of the model**

The two main levers for model calibration were rock permeability and the contour of the temperature iso-surface. This adds an additional challenge to the model calibration process as it requires careful contouring of the basement boundary isotherm along with adjustment of permeability to obtain the geothermal systems in the correct locations and with the correct temperatures.

The final stage of calibration was a temperature matching exercise comparing the calibrated model to the field measurements from 69 wells across the peninsula. Of the 69 wells, temperature data was available from 55% and pressure data from 47% of the wells.

### 5.5 Model results

A vertical slice through the model showing convective plumes for two geothermal systems is shown in Figure 8.

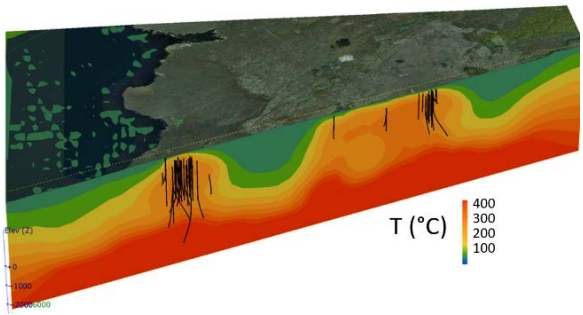


**Figure 8: Vertical slice through the models showing two geothermal systems**

In general, the model provided excellent temperature and pressure matching results, given the resolution of the numerical model within the reservoirs. Many wells shared the same column with one or more other wells and there is no way to differentiate between the different wells without further grid refinement. In most cases this does not cause an issue as wells in a similar location tend to have similar pressure and temperature profiles. Result for well RN24 are shown in Figure 9. Further results are shown in Barton and O'Sullivan (2020).

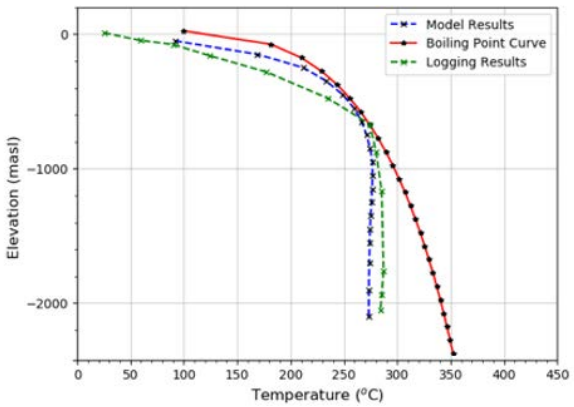


**Figure 9: Temperature profiles for well RN24**

## 6. KRAFLA GEOTHERMAL SYSTEM

Direct evidence of supercritical fluids beneath the Krafla geothermal system in North Iceland was provided by the Iceland Deep Drilling Project well IDDP-1, which encountered a rhyolitic intrusion at ~2.1 km depth and tapped an overlying reservoir of supercritical water at a temperature of 400-500 °C with an enthalpy of ~3.2 MJ/kg (Elders *et al*. 2014). In addition, numerous wells at Krafla have feed-zones below ~2 km with an acid character (Einarsson *et al*., 2010). Chemical and hydrologic modelling suggests that the deep acidic reservoir fluids form an ascending plume of supercritical vapour that condenses during mixing, cooling and depressurization (Heřmanská *et al*., 2019).

A numerical model incorporating the EOS3sc equation-of-state is currently in development. The model is built in Leapfrog, based on previous geologic models developed in Petrel (Weisenberger *et al*., 2015) and GeoModeller (Scott *et al*., 2019). Figure 10 shows a plot of the model grid and rock types at sea level. Consistent with earlier conceptual models of the Krafla system (Bödvarsson *et al*., 1984; Weisenberger *et al*., 2015), deep basement rocks below 1 km depth are separated from shallow high permeability hyaloclastites by a basal lava flow acting as an aquiclude.

Three main types of temperature-depth profiles are observed in the Krafla system: 1) boiling point with depth extending to >2 km depth; 2) a shallow isothermal zone between 0.2-1 km depth, followed by increasing temperatures at greater depths; 3) shallow temperature reversals. The IDDP-1 well is an example of the second category. Figure 11 shows model results for the IDDP-1 well, showing a reasonable match between measured natural state temperatures and model results. Reliable measurements for the IDDP-1 are only available to -1.5 km b.s.l. In this model, a mass generator with an enthalpy of 3.2 MJ/kg was applied to the base of the model at -2.5 km b.s.l, resulting in temperatures in the permeable layer at the base of the well close to 400 °C, consistent with previous models of the IDDP-1 deep reservoir (Axelsson *et al*., 2014). Note that this model is still in development and more results will be published soon.

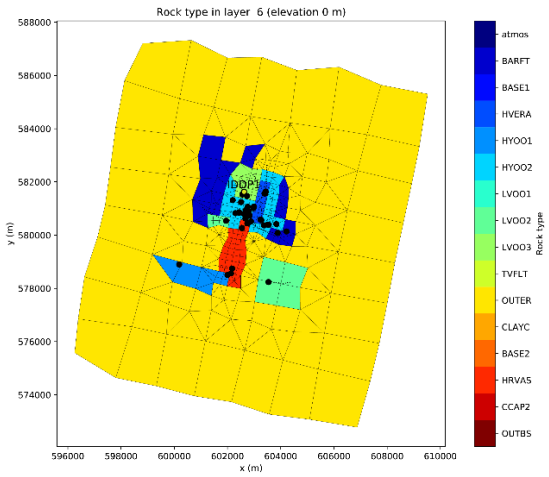


**Figure 10: Model grid and geology at sea level for Krafla.**

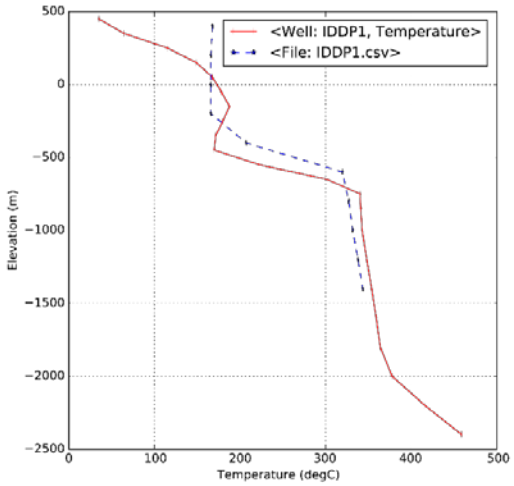


**Figure 11: Comparison between measured natural state temperatures for IDDP-1 (blue dashed line) and model results (red line).**

## 7. TAUPO VOLCANIC ZONE

The final modelling study, based on EOS3sc, is for the Taupo Volcanic Zone (New Zealand). The Taupo volcanic zone (TVZ) is an area of intense volcanism located at the southern end of the Tonga-Kermadec arc, where it intersects mainland New Zealand (Wilson et al., 1995, Wilson and Rowland, 2016). There are 23 highly active geothermal systems (see Figure 12).

The first modelling study of the whole of the TVZ was carried out by Kissling and Weir (2005). Their model covered an area of 150km x 80 km and was 8 km deep. It contained 192,000 elements, each 1 km x 1 km x 0.5 km and was run with the TOUGH2 simulator (Pruess et al., 1999) with a customised supercritical equation of state (Kissling, 2004). Results for surface heat flow at 9 of the major systems (out of a total of 23) were given and for 5 of them the match was good but for the 4 others (Wairakei-Tauhara, Rotokawa, Ohaaki, Rotorua) the match was poor. The model temperatures in the upflow plumes of the geothermal systems were too cold at 200-230°C compared to the measured values of 265-310°C.

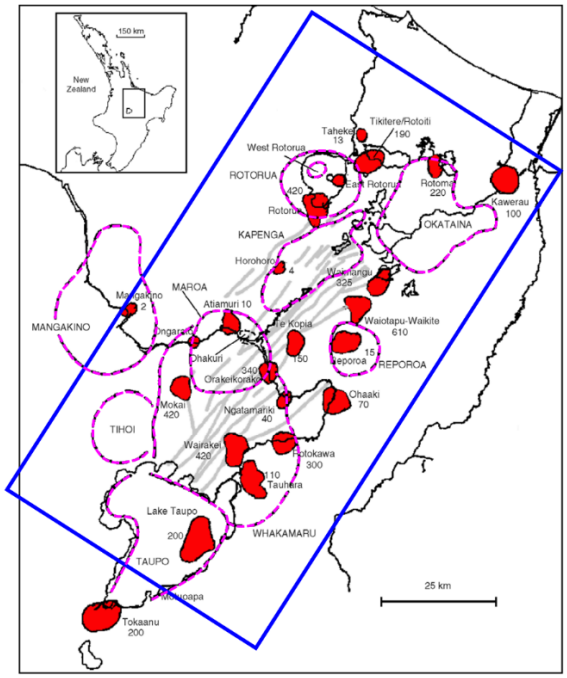


**Figure 12: TVZ geothermal fields (red shaded areas), model extent (blue), Taupo Fault Belt (grey) and volcanic centers (dashed magenta). Modified from Kissling and Weir (2005).**

In a recent paper, Wilson and Rowland (2016) posed the following four questions about the TVZ:

(i). The big picture behind the modern picture – why is there a central TVZ with its accompanying extraordinary geothermal and magmatic fluxes?

(ii). Why is there the spatial separation of geothermal systems and volcanism within the central TVZ and how does it reflect igneous and tectonic processes?

(iii). How stable are the geothermal systems in their positions? Once established, are the systems rooted in the same place?

(iv). How steady are the geothermal systems? Do they wax and wane, and if so, what are the causes for these fluctuations?

Our study addresses (ii)-(iv) (but not (i)) from a modelling rather than geoscientific perspective. We investigate a sequence of models of increasing complexity, looking at the location, heat and mass output and variations in time of the geothermal systems in each case. Most of our models are more general than the flat-topped, fully saturated model of Kissling and Weir (2005) as the top surface follows the topography and we include a shallow unsaturated zone by using the EOS3sc equation-of-state.

The sequence of models we have run are listed in Table 1. All the models cover the same area 128 km x 64 km aligned with the TVZ. Models 1 and 2 have a flat topography, whereas Models 3-8 follow the true topography of the TVZ including the bathymetry of the large lakes. All the models are 7 km deep and the block size is 1 km x 1 km x 0.2 km down to sea level (except for blocks following the topography) and then 1 km x 1 km x 0.5 km below that. For Models 3-8 this results in ~127,000 blocks.

**Table 1: Sequence of models of the TVZ**

| Model | Description |
|---|---|
| 1 | Base-case. Flat topography, two geological layers, uniform heat input across the base |
| 2 | Model 1 with a higher heat flow concentrated in the young TVZ |
| 3 | Model 2 with surface topography applied |
| 4 | Model 3 with basement, volcanic infill and superficial geology included |
| 5 | Model 4 with lower permeabilities outside the young TVZ |
| 6 | Model 5 with large scale structures included (major faults and calderas) |
| 7 | Model 6 with input of magmatic water at the base of the model included |
| 8 | Model 7 with capping structures included |

For the boundary conditions at the top of Models 3-8 dry air was used, with rainfall applied based on average annual rates. In blocks where large lakes are present a wet atmosphere was applied at a pressure corresponding to the approximate average lake depth. Models 1 and 2 used wet atmosphere blocks at 1 bar of pressure. At the bottom boundary a variety of heat flux conditions were applied as described in Table 1. For Models 7 and 8 mass flux was applied at the base of the model to represent additional upflow of magmatic water. The amount was calculated using 14% of the estimated total heat flux for systems in the east and 6% for systems in the west following Giggenbach (1995). The side boundaries were closed.

The geology used in the models was based on the Leapfrog model of the TVZ presented by Alcaraz et al. (2012) and included the basement, volcanic infill and superficial deposits. Major faults and calderas were also included. As described in Table 1, varying levels of geological complexity were included in each of the models.

The model resolution does not allow detailed calibration of individual systems but instead enables investigation of the locations and stability of the systems. As expected, none of the eight models produce a steady state, but rather have systems moving and waxing and waning over time. To account for this, each model was run for 1 million year to allow the model to adjust to its permeability structure and boundary conditions and then the model was run for another 1 million years. At 10,000-year intervals the details of the temperature distributions were extracted and statistics about the number, size, shape and separation of systems were calculated. The distribution and stability of the geothermal systems was then investigated by calculating statistics of how these metrics change over the full simulation of 1 million years.

The temperature distribution for Model 8 at a depth of 500 m averaged over the 1 million years is shown in Figure 13. A comparison of the 200°C contours with the locations of the TVZ geothermal fields shows that a reasonable match to the distribution of geothermal systems can be achieved even with a relatively simple model with coarse resolution.

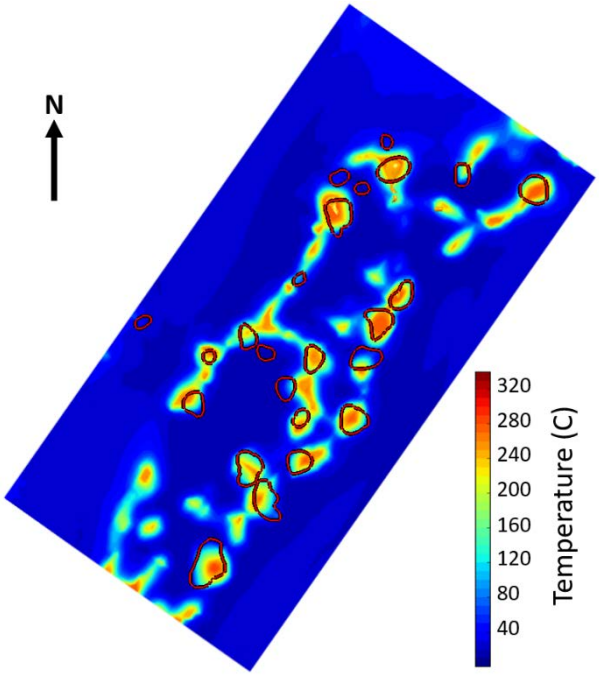


**Figure 13: Average temperature distribution for Model 8 of the TVZ at 500m depth. Location of TVZ geothermal fields indicated with red lines.**

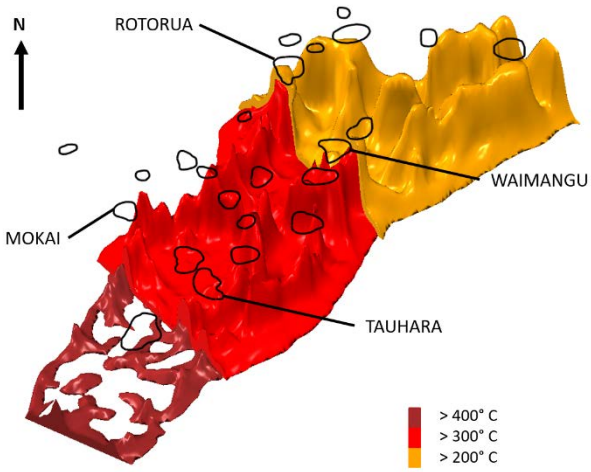


**Figure 14: 3D temperature distribution for Model 8 of the TVZ. The 200°C iso-surface is cut away south of Rotorua-Waimangu and the 300°C iso-surface is cut away south of Mokai-Tauhara. The z-axis is exaggerated by x3. Locations of geothermal fields are indicated with black lines at ground level.**

The smaller, cooler spots also indicate the locations where smaller hot plumes evolve and decay during the 1 million-year simulation, demonstrating the inherent transient nature of the model.

Figure 14 shows the 3D temperature distribution of Model 8 for a typical timestep during the simulation. The 200°C and 300°C isotherms are cut away at different locations to show the distribution of the high temperatures beneath. The plot shows the complexity of the temperature distribution and the presence of many deep, small, high temperature plumes in the model. Note the z-axis is exaggerated by a factor of 3.

The main conclusions of the study from a modelling perspective are that the locations of the zones where geothermal systems form are controlled largely by a combination of the location of the deep, high heat flow and the surface topography. But the size and shape of individual systems and the separation between them is controlled more by the heterogenous permeability distribution and the formation of the capping structures.

## 8. CONCLUSION

The modification we have made to EOS1sc and EOS3sc, the supercritical equations-of-state for TOUGH2, allow them to work well for natural state simulations of complex geothermal systems. This has enabled the calibration of full-scale models of two high temperature geothermal systems and two very large regional models including multiple geothermal systems. Having a robust, reliable tool for simulating supercritical geothermal conditions paves the way for carrying out detailed investigations of the deep roots of geothermal systems, thus helping to understand how multiple systems interact and helping in the investigation of the potential for locating and utilizing deep geothermal resources.

## ACKNOWLEDGEMENTS

All the projects described in this paper made extensive use of Leapfrog Geothermal and the authors gratefully acknowledge the support of Seequent for making research licenses available.

## REFERENCES

Alcaraz, S.A., Rattenbury, M.S., Soengkono, S., Bignall, G., Lane, R.: A 3D Multi-Disciplinary Interpretation of the Basement of The Taupo Volcanic Zone, New Zealand, *Proc. 37th Workshop on Geothermal Reservoir Engineering*, Stanford University, Stanford, CA, (2012).

Axelsson, G., Egilson, T., Gylfadóttir, S.: Modelling of temperature conditions near the bottom of well IDDP-1 in Krafla, Northeast Iceland. *Geothermics*, 49, 49–57 (2014).

Baraza, R.O., O'Sullivan, J.P.: An Integrated Leapfrog/AUTOUGH2-SC Model of the Menengai Geothermal Field. Accepted for *Proc. 8th African Rift Geothermal Conference*, Nairobi, Kenya (2020).

Barton, S.A. and O'Sullivan, J.P.: Combined conceptual and supercritical numerical model of the Reykjanes peninsula. Accepted for *Proc. World Geothermal Congress 2020* (originally scheduled to be held in Reykjavik, Iceland) (2020).

Bödvarsson, G., Pruess, K., Stefánsson, V., Eliasson, E. T.: The Krafla geothermal field, Iceland 2. The natural state of the system. *Water Resources Research,* 20, 1531–1544 (1984).

Brazhkin, V.V., Trachenko, K.: What separates a liquid from a gas? *Physics Today*, 65, 11, 68 (2012).

Brikowski, T.H.: Modeling supercritical systems with TOUGH2: preliminary results using the EOS1SC equation of state module, *Proc. 26th Workshop on Geothermal Reservoir Engineering*, Stanford University, Stanford, CA, (2001).

Croucher, A.E., O'Sullivan, M.J.: Application of the computer code TOUGH2 to the simulation of supercritical conditions in geothermal systems, *Geothermics*, **37**, 622-634 (2008).

De Freitas, M.A. et al.: Numerical simulation of the Svartsengi geothermal field, SW-Iceland. Presented at United Nations University, Geothermal Training Programme, *40th Anniversary Workshop*, Reykjavik, April 26 (2018).

Einarsson,K., Pálsson, B., Gudmundsson, A., Hólmgeirsson, S., Ingason, K., Matthíasson, J., Hauksson, T., Ármannsson, H.: Acid Wells in the Krafla Geothermal Field. *Proc. World Geothermal Congress 2010*, Bali, Indonesia (2010).

Elders, W.A., Nielson, D., Schiffman, P., Schriener, Jr.: A. Investigating ultra-high enthalpy geothermal systems: a collaborative initiative to promote scientific opportunities. *Scientific Drilling*, 2, 1-8 (2014).

Driesner, T., Weis, P., Scott, S.: A New Generation of Numerical Simulation Tools for Studying the Hydrology of Geothermal Systems to "Supercritical" and Magmatic Conditions, *Proc. World Geothermal Congress 2015*. Melbourne, Australia (2015).

Giggenbach, W.F. (1995). Variations in the chemical and isotopic composition of fluids discharged from the Taupo Volcanic Zone, New Zealand. *J. Volcanology Geothermal Research*, **68**, 89-116.

Hayba, D.O., and Ingebritsen, S.E.: *The Computer Model HYDROTHERM, a Three-Dimensional Finite-Difference Model to Simulate Ground-Water Flow and Heat Transport in the Temperature Range of 0–1200*℃. U.S. Geological Survey Water Resources Investigation 94-4045, Reston, VA (1994).

Heřmanská, M., Stefánsson, A., Scott, S. Supercritical fluids around magmatic intrusions: IDDP-1 at Krafla, Iceland. *Geothermics*, 78, 101–110 (2019).

Kanda, I., Fujimitsu, Y., Nishijima, J.: Geological structures controlling the placement and geometry of heat sources within the Menengai geothermal field, Kenya, as evidenced by gravity study. *Geothermics*, 79, 67-81 (2019).

Khodayar, M., Björnsson, S., Guðnason, E. Á., Níelsson, S., Axelsson, G., Hickson, C.: Tectonic control of the Reykjanes geothermal field in the oblique rift of SW Iceland: From regional to reservoir scales. *Open Journal of Geology*, 8(03), 333 (2018).

Kipyego, E., O'Sullivan, J. and O'Sullivan, M.: An initial resource assessment of the Menengai caldera geothermal system using an air-water TOUGH2 model, *Proc. 35th New Zealand Geothermal Workshop*, Rotorua, New Zealand (2013).

Kissling, W.M., (PhD thesis): *Deep Hydrology of the Geothermal Systems in the Taupo Volcanic Zone*, New Zealand, University of Auckland, New Zealand (2004).

Kissling, W. M., Weir, G.J.: The spatial distribution of the geothermal fields in the Taupo Volcanic Zone, New

Zealand. *J. Volcanology Geothermal Research*, 145, 136–150 (2005).

Klyukin, Y., Driesner, T., Steele-MacInnis, M., Lowell, R. P., Bodnar, R. J.: Effect of salinity on mass and energy transport by hydrothermal fluids based on the physical and thermodynamic properties of H2O-NaCl. *Geofluids*, 16, 585–603 (2016).

Leat, P.T.: Geological Evolution of the Trachytic Caldera Volcano Menengai, Kenya rift Valley, *J. Geological Society*, 141, 1057-1069 (1984).

Magnusdottir, L., Finsterle, S.: An iTOUGH2 equation-of-state module for modeling supercritical conditions in geothermal reservoirs. *Geothermics*, 57, 8-17 (2015).

O'Sullivan, J.P., Croucher, A., Yeh, A., O'Sullivan, M.J.: Improved Convergence for Air-Water and CO2-Water TOUGH2 Simulations, *Proc. 35th New Zealand Geothermal Workshop*, Rotorua, New Zealand (2013).

O'Sullivan, J.P., Croucher, A., Yeh, A., O'Sullivan, M.J.: Further Improvements in the Convergence of TOUGH2 Simulations, *Proc. 6th European Conference on Computational Fluid Dynamics*, Barcelona, (2014).

O'Sullivan, J., Kipyego, E., Croucher, A., Ofwona, C., O'Sullivan, M.: A Supercritical Model of the Menengai Geothermal System, *Proc. World Geothermal Congress 2015*, Melbourne, Australia (2015).

O'Sullivan, J., O'Sullivan, M., Croucher, A.: Improvements to the AUTOUGH2 supercritical simulator with extension to the air-water equation-of-state. *Geothermal Resources Council Transactions*, 40, 921-929 (2016).

Pritchett, J.W.: STAR: a geothermal reservoir simulation system, *Proc. World Geothermal Congress 1995*, Florence, Italy (1995).

Pruess, K., Oldenburg, K., Moridis, G.: *TOUGH2 User's Guide, version 2.0*, Lawrence Berkeley National Laboratory, Berkeley, California. (1999).

Scott, S., Driesner, T., Weis, P.: Hydrology of a Supercritical Flow Zone Near a Magmatic Intrusion in the IDDP-1 Well – Insights from Numerical Modeling, *Proc. World Geothermal Congress 2015*, Melbourne, Australia (2015a).

Scott, S., Driesner, T., Weis, P.: Geologic controls on supercritical geothermal resources above magmatic intrusions. *Nature Communications*, 6, 7837 (2015b).

Scott, S., Driesner, T., Weis, P.: The thermal structure and temporal evolution of high-enthalpy geothermal systems. *Geothermics*, 62, 33–47 (2016).

Scott, S., Driesner, T., Weis, P.: Boiling and condensation of saline geothermal fluids above magmatic intrusions. *Geophys. Res. Lett.*, 44, 1–10 (2017).

Scott, S. W. *et al.* A probabilistic geologic model of the Krafla geothermal system constrained by gravimetric data. *Geothermal Energy*, **7**, (2019).

Wagner, W., Cooper, J.R., Dittman, A., Kijima, J., Kretzschmar, H.-J., Kruse, A., Mares, R., Oguchi, K., Sato, H., Stöcker, I., Sifner, O., Takaishi, Y., Tanishita, I., Trübenbach, J., Willkommen, Th.: The IAPWS Industrial Formulation 1997 for the thermodynamic properties of water and steam. *ASME J. Eng. Gas Turbines Power*, 122, 150–182 (2000).

Weis, P., Driesmer, T., Coumou, D., Geiger, S.: Hydrothermal, multiphase convection of H2O-NaCl fluids from ambient to magmatic temperatures: a new numerical scheme and benchmarks for code comparison. *Geofluids*, 14, 347-371, (2014).

Weisenberger, T. B. *et al*.: *Revision of the Conceptual Model of the Krafla Geothermal System*. Iceland Geosurvey Report LV-2013-02 (2015).

Wilson, C.J.N., Houghton, B.F., McWilliams, M.O., Lanphere, M.A., Weaver, S.D., Briggs, R.M.: Volcanic and structural evolution of Taupo Volcanic Zone, New Zealand: a review. *J. Volcanology Geothermal Research*, 68, 1–28 (1995).

Wilson, C.J.N., Rowland, J.V.: The volcanic, magmatic and tectonic setting of the Taupo Volcanic Zone, New Zealand, reviewed from a geothermal perspective. *Geothermics*, 59, 168–187 (2016).

Yeh, A., Croucher, A., O'Sullivan, M.J.: Recent developments in the AUTOUGH2 simulator, *Proc. TOUGH Symposium 2012*, Berkeley, California, September 17-19, (2012).


ISSN 2703-4275